Accounting for Surface Wave Distortion of the Marine Wind Profile in Low-Level Ocean Storms Wind Measurements

W. G. LARGE, J. MORZEL, AND G. B. CRAWFORD*

National Center for Atmospheric Research,† Boulder, Colorado

(Manuscript received 2 March 1994, in final form 1 July 1994)

ABSTRACT

Marine wind measurements at three heights (3.0, 4.5, and 5.0 m) from both moored and drifting buoys during the Ocean Storms Experiment are described. These winds are compared with each other, with winds from ships, from subsurface ambient acoustic noise, and from the analyses of three numerical weather prediction centers. In the mean, wind directions generally differ by only a small constant offset of a few degrees. No wave influence on the wind direction is evident, because the differences are not systematic and, with few exceptions, they are less than the expected error. After correcting for some apparent calibration and instrument bias, the Ocean Storms wind speeds display similar behavior when compared to the analyzed wind products. There is excellent agreement up to a transition wind speed between 7 and 10 m s^{-1}, above which all the measured winds tend to be relatively low. The transition speed is found to increase with anemometer height, so this behavior is interpreted as being due to the distortion of the wind profile by surface waves. The wave effects are shown to be profound. By increasing the stress by 40% or more in high winds, the corrections are shown to be essential for numerical models to simulate the oceanic response to storm events. The Ocean Storms corrections are used to construct functions describing wave influence on both the vertical wind shear and the mean wind speed profile. These functions can only be regarded as crude approximations because the Ocean Storms data are far from ideal for determining them. However, they can be used to assess potential influences of surface waves on any low-level wind measurement.

1. Introduction

Marine winds are often measured by buoy-mounted anemometers at heights, z_a, only a few meters above the sea surface (e.g., Weller et al. 1990). Such observations are used for a variety of purposes. They are often transmitted in real time to the operational numerical weather prediction centers for incorporation into their global analyses (e.g., Lorenc 1981). They are commonly used as ground truth for satellite wind retrievals (e.g., Jones et al. 1982; Halpern et al. 1994). Buoy winds are also used to establish the wind forcing of the upper ocean on a variety of timescales. This forcing can then be used in the analysis and interpretation of ocean observations (e.g., Price et al. 1987) or can be applied to numerical ocean models (e.g., Large and Crawford 1995).

Most uses of marine winds involve either explicit or implicit calculation of the wind stress through the bulk aerodynamic method. This method requires that wind observations be shifted to the standard reference height, z_s = 10 m, where the drag coefficient has been formulated. Shifting the wind from z_a to z_s, in turn, requires knowledge of the wind profile. However, marine wind profiles are known to be distorted from their familiar logarithmic dependency by both the atmospheric stability and by ocean surface waves. The former effect has been quantified (Deardorff 1968) and is usually accounted for (Large and Pond 1981). On the other hand, surface wave distortion is not well understood and is almost always neglected, even though Dittmer (1977) shows that it can be significant even in relatively benign tropical conditions. He shows marine wind profiles from a stabilized spar buoy, where the mean speeds from 2-m height are systematically too low with wave heights less than 0.75 m. Another example from the JONSWAP II experiment in the German Bight is given by Krugermeyer et al. (1978). They conclude that the wave influence on the wind profile may extend to about three wave heights.

The distortion of the wind profile above surface waves has been used to explain the observed systematic discrepancy between wind stresses inferred from observed profiles and coincident stresses obtained from the eddy correlation technique (Dittmer 1977). The

* Current affiliation: College of Oceanic and Atmospheric Sciences, Oregon State University, Corvallis, Oregon.

† The National Center for Atmospheric Research is sponsored by the National Science Foundation.

Corresponding author address: Dr. William G. Large, National Center for Atmospheric Research, 1850 Table Mesa Drive, P.O. Box 3000, Boulder, CO 80303.

wind-wave tank results of Tseng et al. (1992) can be interpreted in a similar fashion, even though they formulate the problem in terms of the height of the zero reference plane for the wind profile, which they conclude must vary with wave conditions. Theoretical considerations of wind generation of ocean surface waves require that the waves distort the wind profile, but Janssen (1989) predicts that even in strong winds the effect extends only to about 5-cm height.

In the Ocean Storms Experiment of 1987, most of the wind observations were made from moored and drifting buoys at heights of 4.5 and 3.0 m, respectively. It is expected that these heights would sometimes be comparable to the wave height because high winds are common in the Ocean Storms region. This paper addresses the question of how to account for the distortion of the wind profile by the surface waves when deriving wind stress from these low-level wind observations.

2. The marine wind profile

In the atmospheric surface layer, it is conventional to align the downstream wind component, U, with the x axis of a Cartesian coordinate system. This surface layer is not a constant stress layer (Tennekes 1973) but still can be defined as the turbulent flow regime where the only important dimensional parameters are the density ρ, the height above the boundary z, the surface wind stress τ_0, and the surface buoyancy flux B_0. Two fundamental turbulence parameters that can be formed from these quantities are the friction velocity u^* and the Monin–Obukhov length scale L:

$$u^{*2} = |\tau_0|/\rho$$
$$L = u^{*3}(\kappa B_0)^{-1}, \tag{1}$$

where $\kappa = 0.4$ is the von Kármán constant. The semi-empirical Monin–Obukhov similarity theory then gives the well-tested wind flux profile relation as a function of the stability parameter, $\zeta = z/L$:

$$\phi(\zeta) = \frac{\kappa z}{u^*}\frac{\partial U}{\partial z}. \tag{2}$$

This function (2) has been empirically determined (Högström 1988). Integration of (2) leads to the familiar logarithmic wind profile with corrections for stability:

$$U(z) = U_0 + \frac{u^*}{\kappa}\left[\ln\left(\frac{z}{z_0}\right) - \psi(\zeta)\right], \tag{3}$$

where

$$\psi(\zeta) = \int_{z_0/L}^{\zeta} \frac{[1-\phi(\zeta')]}{\zeta'}\, d\zeta'.$$

The constant of integration, z_0, is the roughness length defined as the height at which a wind profile governed by (2) would match the surface flow; that is, $U(z_0) = U_0$.

Tennekes (1973) gives an alternative derivation of (3) and discusses the extent of the atmospheric surface layer. A practical definition is the height where the wind stress has been reduced by 20% from its surface value (Lumley and Panofsky 1964). In midlatitudes this height, z_2, scales as $A_2 U(z_s)$, with $A_2 \approx 5.5s$, in steady winds. It is higher (lower) when the wind speed is increasing (decreasing) with time (Large 1979; Danard 1980).

The bottom of the atmospheric surface layer at $z = z_1$ is where the surface roughness elements begin to directly influence the turbulent flow. If over the sea the roughness elements are the surface waves, then z_1 would scale with the wave height. Neither (2) nor (3) can be expected to hold for $z < z_1$. Dimensional analysis suggests that a possible model for the structure of the mean wind profile at these heights is

$$\chi(\xi)\phi(\zeta) = \frac{\kappa z}{u^*}\frac{\partial U}{\partial z}, \tag{4}$$

where $\xi = z/h$, with h an unknown wave height parameter, and χ is an unknown function still to be determined empirically. At large values of ξ, χ should approach a value of 1, so that (4) becomes (2) making (3) valid. The profiles of Dittmer (1977) indicate that at smaller ξ, χ should become greater than 1.

High marine winds are typically accompanied by high waves and near-neutral conditions (ζ near zero, ϕ about 1). In such cases (4) can be integrated analogously to (2) to give the logarithmic wind profile as distorted by surface waves:

$$U(z) = U_0 + \frac{u^*}{\kappa}\left[\ln\left(\frac{z}{z_r}\right) - \Omega(\xi)\right], \tag{5}$$

where

$$\Omega(\xi) = \int_{\xi_r}^{\xi} \frac{[1-\chi(\xi')]}{\xi'}\, d\xi'$$

and $\xi_r = z_r/h$. The roughness length z_r is the height where the wind from (5) and the surface speed are equal [$U(z_r) = U_0$].

An example of the possible neutral wind profiles given by (5) and (3), with $U_0 = 0.0$ and $U(z_s) = 13.0$ m s^{-1}, as shown in Fig. 1. In this case z_1 is assumed to be about 7.0 m and higher up, where the physics of both (2) and (4) are valid, the two profiles coincide. Lower, the larger wind gradient results in lower wind speeds from (5) than from (3), and z_r is nearly three orders of magnitude larger than z_0. The actual wind profile would be expected to follow (5) (solid trace) only so far as no other physical parameters become important and (4) remains valid. At these heights, Fig. 1 is qualitatively similar to the model of Chalikov and Makin (1991). Figure 1 also illustrates that if an ane-

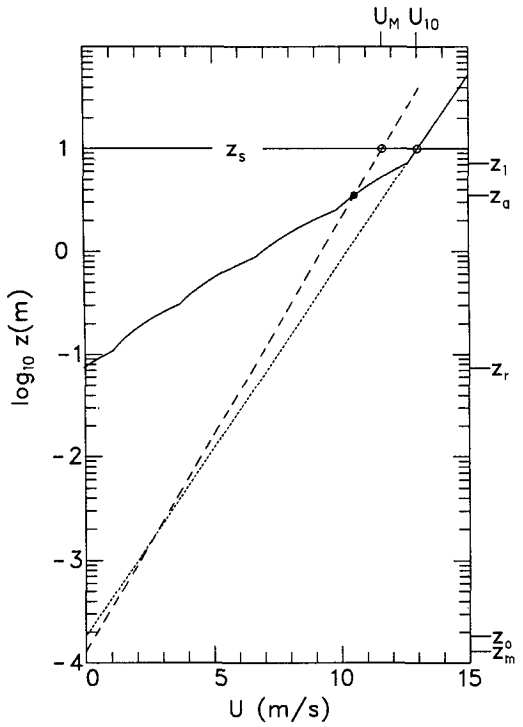

FIG. 1. Schematic of a neutral low-level wind profile with U_{10} = 13.0 m s^{-1} as predicted by (5), solid trace, and (3), dotted trace. The dashed trace shows (3) as derived from an anemometer measurement at z_a below the surface layer ($z_a < z_1$). These three profiles go to zero at z_r, z_0, and z_m, respectively.

mometer at z_a = 3.5 m measures the correct wind speed U_a, which is then shifted to a neutral 10-m value U_M according to (3), this inferred value would be significantly less than the true neutral 10-m speed U_{10}.

The bulk aerodynamic formula for computing the surface wind stress, and hence u^*, from measurements of the wind is

$$\boldsymbol{\tau}_0 = \rho C_D(z, \zeta) U(z) \mathbf{U}(z), \tag{6}$$

where the drag coefficient C_D is a function of height and stability. In formulating C_D it is common to reference it to a height of z_s = 10 m and to neutral stability ($\zeta = 0$):

$$C_N = C_D(z_s, 0) = \frac{|\boldsymbol{\tau}_0|}{\rho U_{10}^2} = \left(\frac{u^*}{U_{10}}\right)^2. \tag{7}$$

A very good fit to published data averaged over wind speed bins from 1 to more than 25 m s^{-1} (E. Vera 1983, unpublished manuscript) is

$$u^{*2} = 10^{-3}[2.717U_{10} + 0.142U_{10}^2 + 0.0764U_{10}^3]. \tag{8}$$

With the formulation implied by (8), C_N goes to its theoretical infinite limit at zero wind speed, and significantly increases with wind speed for $U_{10} > 10$ m s^{-1}. This increase results in a measured roughness length z_m smaller than z_0 (Fig. 1).

In computing the data used in the fit (8), U_{10} at best has been calculated using (3), ignoring any surface wave influence (e.g., Large and Pond 1981). Thus, when measurements of stress and wind speed have been made in high wind/wave conditions with $z_2 > z_a > z_1 > z_s$, the estimate of $U(z_s)$ used to compute C_N has been a smooth sea value rather than the smaller actual wave influenced speed (Fig. 1, dotted versus solid curves). The C_N values implied by (7) and (8), therefore, are referenced also to a smooth sea, as well as to neutral stability and to 10-m height. They should result in good bulk stress estimates (6) provided the wind measurements were made at heights above the wave influence, $z_a > z_1$. Figure 1 illustrates that inferred winds U_M from low-level anemometers and (3) could result in bulk stress magnitudes that are much too low. Instead, (5) should be used, which requires an estimate of ξ and the empirical determination of $\Omega(\xi)$.

We note that drag coefficients C_N derived from (3) and measurements of stress and wind at heights $z_a < z_1$ would be systematically larger than the smooth sea values. Thus, measurement height could explain some of the differences from dataset to dataset in reported drag coefficients.

3. The Ocean Storms wind observations

The wind observations considered in this study are cataloged in Table 1. Figure 2 shows the locations of the five surface moorings. Two of these, the Ocean Storms central, S_C, and north, S_N, moorings, were deployed specifically for Ocean Storms and operated from August 1987 to June 1988. Propeller–vane anemometers were installed at a height of 4.5 m. The other three moorings are part of the offshore NOAA operational network run by the National Data Buoy Center (NDBC). These buoys have boat-shaped hulls, 6 m long by 3 m wide. They also have propeller–vane anemometers, but at z_a = 5.0 m. Their reported winds are vector averages over 8.5-minute intervals from 1 Hz samples.

The drifting wind observations were made along the tracks shown in Fig. 2. Each of the six Climate Air–Sea Interaction Drifting (CASID) buoys (C_0 to C_5) employed a propeller–vane anemometer at 3.0-m height. All buoys were deployed early in October, but only one, C_3, continued to operate into the new year.

In pilot experiments a CASID was additionally instrumented to measure the three components of acceleration, as well as buoy pitch and roll. The results indicated that periods of excessive buoy motion lasted for only about 10 seconds and were accompanied by widely varying vane activity. Thus, anomalous wind directions were indicative of an overly active buoy and unreliable wind samples. To exclude such periods from the Ocean Storms observations, the CASID wind pro-

cessing was as follows. Five minute (300 samples) blocks of wind speed data were internally processed. Only samples whose wind direction were within ±30° of the most common direction were used to compute a simple mean speed and direction for a block. Typically only 10%–15% of the samples were excluded. Then, to conserve power, the buoy system was muted for about 4.5 minutes before new block means were computed. Every 1.3 hours, eight-block means were vector averaged to give the wind speed and direction data that were transmitted to the Argos satellite data collection system.

The two French Marisonde drifters (M_3 and M_7) were also deployed early in October, but failed relatively soon. These drifters used Savonius rotor wind speed sensors at about 3.0-m height. A large fin was rigidly attached to the buoy hull, and the orientation of the hull was used to give the wind direction.

At various times the CSS *Parizeau* operated in the vicinity of the Ocean Storms moorings. Wind measurements from a cup and vane system at about 19 m were continuously recorded and are denoted as P_C (Table 1). In addition, fast response propeller–vane anemometers were installed at about 9 m on a mast at the ship's bow and at about 15 m near the ship's bridge. These *Parizeau* winds did not operate continuously and are denoted in Table 1 as P_M and P_B, respectively. Periodically, a small drifting buoy, denoted P_D, was deployed from the *Parizeau* with a cup and vane anemometer at about 3.0-m height.

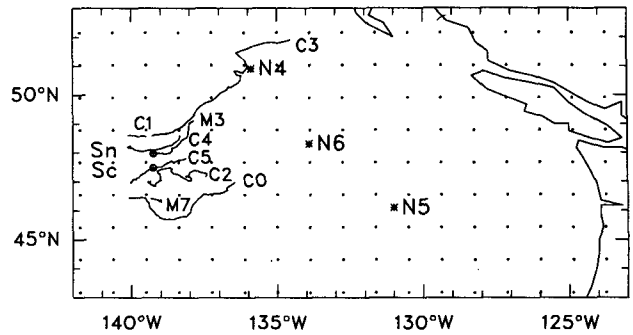

FIG. 2. Locations of Ocean Storms wind observations that are cataloged in Table 1. The dots correspond to the approximately 1° grid of the ECMWF-analyzed products.

An unconventional wind speed dataset was provided throughout Ocean Storms by a Wind Observations Through Ambient Noise (WOTAN) instrument on a subsurface mooring near the central mooring. This device measured acoustic noise (4–20 kHz) at 150-m depth. The noise measurements were converted to 10-m wind speeds using an algorithm of Vagle et al. (1990), which was based on measurements during the earlier Frontal Air–Sea Interaction Experiment (FASINEX). The FASINEX winds used in this calibration were from a Gill 3-cup anemometer at 3.55-m height on a mooring (Weller et al. 1990). Most of these calibration data were at wind speeds below 10 m s^{-1}. At

TABLE 1. Ocean Storms wind observing systems and suggested corrections, $\delta\theta$. Asterisks denote platforms that transmit their winds to the operational forecast centers for incorporation into their analyses.

Platform		Wind sensor	z_u (m)	$\delta\theta$ (°)	
Mooring	S_C	Prop-vane	4.5	−1	Storms central
	S_N	Prop-vane	4.5	0	Storms north
	N_{4*}	Prop-vane	5.0	−1	NDBC 46004
	N_{5*}	Prop-vane	5.0	5	NDBC 46005
	N_{6*}	Prop-vane	5.0	10	NDBC 46036
Drifter	C_0	Prop-vane	3.0	−5	CASID 10060
	C_1	Prop-vane	3.0	5	CASID 10061
	C_2	Prop-vane	3.0	0	CASID 10062
	C_3	Prop-vane	3.0	−4	CASID 10063
	C_4	Prop-vane	3.0	0	CASID 10064
	C_5	Prop-vane	3.0	3	CASID 10065
	M_3	Rotor-fin	3.0	5	Marisonde 33
	M_7	Rotor-fin	3.0	0	Marisonde 37
	P_D	Cup-vane	3.0	−30	Parizeau drifter
Ship	P_{C*}	Cup-vane	18.9		Parizeau
	P_M	Prop-vane	9.0		Parizeau bow mast
	P_B	Prop-vane	15.0		Parizeau bridge
Subsurface	W_C	WOTAN	−150	—	Near-storms central
Analyses	EC		10.0	1	ECMWF, 6 hourly
	NM		10.0	5	NMC, 12 hourly
	FN		10.0	0	FNOC, 12 hourly

higher wind speeds the calibration is essentially an extrapolation from the lower speeds.

Valuable meteorological datasets, including 10-m wind speed and direction, were obtained from the analysis products of three operational numerical weather forecast centers. The European Centre for Medium-Range Weather Forecasts (ECMWF) provides global fields every 6 hours on the approximately 1-degree grid shown by the dots in Fig. 2. Air and dewpoint temperatures at 2-m height are also in the dataset. Similar products from a similar procedure, but on a coarser 2-degree grid, are provided every 12 hours by both the National Meteorological Center (NMC) and the Fleet Numerical Oceanography Center (FNOC). All three datasets are available throughout Ocean Storms, and for comparison purposes these data were interpolated to the time and positions of other Ocean Storms observations.

In 1987 the ECMWF data assimilation (Lorenc 1981) included a global, multivariate, optimal interpolation analysis. The observational data, including that indicated in Table 1, underwent three quality control checks (Hollingsworth et al. 1986). First, they were compared to the first guess from a previous forecast and excluded if too different. Next, a univariate check was applied to nearby observations to identify redundancies. Finally, they were compared to an independent analysis using neighboring observations. The 10-m wind components and the 2-m temperatures were calculated by integrating profiles of the gradients (2), assuming a constant flux (surface) layer and a Charnock constant of 0.018 (ECMWF 1993). The 2-m dewpoint was computed assuming a constant relative humidity in the surface layer.

For buoy and mooring intercomparisons, the wind data were averaged over or interpolated to 1-hour intervals. For comparisons with the much larger scale analyzed winds, wind data buoy and mooring data were averaged over 6 hours. All the wind speeds were shifted to a common reference height, $z_s = 10$ m, using (3) and (8). Most wind measurements were accompanied by air and sea temperature measurements, so the surface buoyancy flux B_0 in (1) and hence ζ could be estimated and the effects of atmospheric stability taken into account. Any missing temperature or humidity data were supplied by interpolating the ECMWF data in both time and space. Thus, the wind speeds that are to be compared have been corrected for measurement height differences and atmospheric stability, but they still retain any wave distortion effects.

4. Wind directions

All wind directions θ are defined to be in the direction of the wind stress, the direction to which the wind is blowing, and are given as degrees clockwise from true north. In comparing wind direction datasets, one is chosen to be the independent variable, θ_x, and another the dependent, θ_y. The mean difference $\Delta\theta$ and standard deviation σ of complete comparative datasets of N points are computed as

$$\Delta\theta = \frac{1}{N}\sum(\theta_x - \theta_y)$$

$$\sigma^2 = \frac{1}{(N-1)}\sum(\theta_x - \theta_y)^2. \tag{9}$$

To obtain a more representative estimate of mean differences, outliers were eliminated by following an iterative procedure. For the ith iteration a subset of N_i points is chosen such that, for all points,

$$\theta_x - (\theta_y + \Delta\theta_{i-1}) \leqslant 30° \tag{10}$$

from which a mean difference $\Delta\theta_i$ and standard deviation σ_i are computed following (9). For the first iteration $\Delta\theta_0 = 0.0$ is used. In practice, one iteration is usually sufficient, because the Ocean Storms wind directions are in very good agreement, differing by only small offsets.

All measurements of wind direction rely upon a compass reading, and most also require a vane heading. The two major sources of error are likely the alignment of the vane reference with the compass lubber line and the calibrations of both compass and vane. Drifting buoy assembly is such that it is difficult to achieve alignment to better than ~5°. Vane calibration can be more accurate, but together with that of the compass, another 5° uncertainty is due to calibration. The total system accuracy of the NDBC wind directions, for example, is reported to be ±10° (Gilhousen et al. 1990). Therefore, any two wind direction datasets that differ by less than 5° in the mean should be regarded as being in agreement.

Figure 3 is a scatterplot of interpolated ECMWF (θ_y) versus the central mooring (θ_x) wind directions. Winds with a westerly component $0° < \theta < 180°$ are most common, while winds from the northeast ($\theta = 225°$) are rare. There are some cases, usually associated with low wind speeds, where the directions are very different. Large differences at high wind speeds are also expected when the mooring is located on one side of a real front and on the other side of the model front. After the largest of these outliers (about 10% of the data) are excluded according to (10), the only major difference in the two datasets is a small offset. The mean difference, $\Delta\theta_1$, is only 2.3°, so the two sets of measurements agree.

The results of the primary Ocean Storms wind direction comparisons are cataloged in Table 2. The first group shows the central mooring to analyses comparisons. The ECMWF to S_C comparison of Fig. 3 is typical. The agreement between FNOC and S_C is best in the mean, but the scatter is the largest of this group.

In the second group of Table 2, ECMWF directions are compared to those from Ocean Storms drifters.

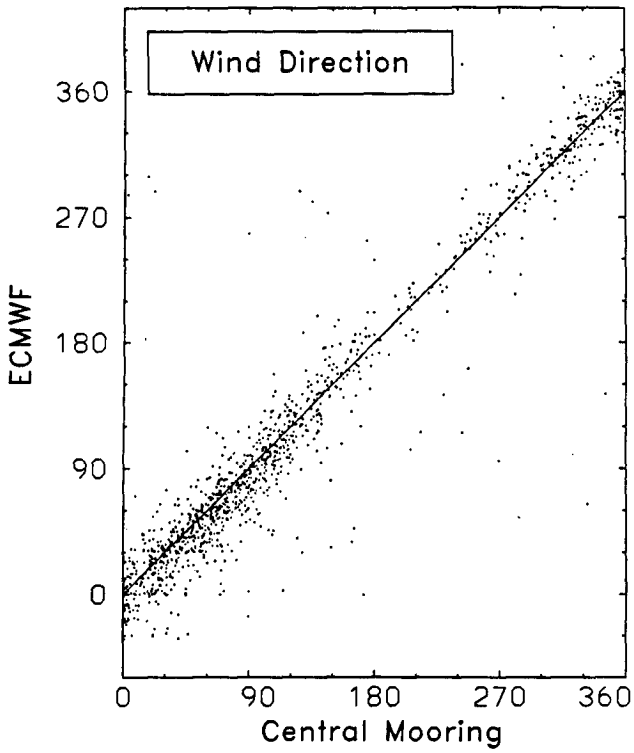

FIG. 3. Scatterplot of interpolated wind directions from ECMWF vs the reported wind directions from the central mooring. The 1:1 line of perfect agreement is shown for reference.

Larger than expected mean differences are found only for the *Parizeau* drifter, P_D, and M_3, with $\Delta\theta = -31°$ and 20°, respectively. The other drifters, including all six CASID buoys, show good agreement in the mean. However, there were only $N = 34$, $N_1 = 21$ observations from M_7 for comparison, and the resulting $\sigma = 57$ is the largest scatter of any comparison. An important result is that the observed differences, especially between the identical CASID buoys, are not systematic.

Results from the third group of comparisons (S_C to drifters) are generally consistent with the findings of the first two groups. Only data from periods when a drifter was within 150 km of the central mooring are included in these comparisons. Again the Marisonde and *Parizeau* drifters compare least favorably. The S_C wind directions appear to differ from each CASID by only a small offset. The two Ocean Storms moorings, S_C and S_N, were about 60 km apart, yet the mean direction difference is less than a degree.

Table 2 (group 4) also shows the interpolated ECMWF to NDBC buoy wind direction comparisons. Buoy N_6 gives the largest mean difference, but there are few data points. Both N_4 and N_5 have many more points and give mean differences well within their claimed system accuracies.

In addition, numerous secondary comparisons of wind direction were made. For example, all the drifting buoys were intercompared with each other and with the north mooring, using data from times when measurements were separated by less than 100 km. These results were qualitatively similar to those of the primary comparison. Mean differences tended to have consistent signs, but the amounts varied by a few degrees.

In summary, most of the wind datasets can be made to agree with each other in mean direction to within a few degrees by applying small constant corrections. A very consistent direction dataset can be constructed by adding the $\delta\theta$ corrections of Table 1 to each dataset. A lot of data appears to fall between the S_C and ECMWF directions, so 1° is added to the ECMWF directions and 1° is subtracted from the S_C. No corrections are then required for the S_N mooring and for the C_2, C_4, and M_7 drifters, nor for the FNOC analyses. Only small corrections of ±5° are needed for the NMC analysis and for all the other platforms with two exceptions. The small N_6 dataset suggests that about 10° should be added to its reported direction. The *Parizeau* drifter seems to have been seriously in error, requiring about a −30° correction. The M_3 directions are useful only if about half are rejected according to (9). The remainder need to be corrected by about 5°.

5. Wind speeds

The results to be presented in this section suggest that flow distortion extended beyond the anemometer heights in high wind/wave conditions. As a result the computed 10-m wind speeds from (3) are underestimated in such conditions, even though the low-level winds themselves appear to be consistent and accurately measured by most of the moorings and drifters. Furthermore, it will be shown that the resulting error in computed wind stress is serious.

The small dots of Fig. 4 are a scatterplot of the wind speeds from ECMWF versus central mooring wind speeds from August 1987 to June 1988. The averages (circles) in Fig. 4 and those in subsequent plots are bin averages. Each bin is bounded by lines perpendicular to the solid 1:1 line at 2 m s^{-1} increments along the line. Averages from bins with less than 6 points are never plotted. At wind speeds below about $U^L = 3$ m s^{-1}, the implicit spatial average of the analysis and the 6-hour time average of the mooring may not be comparable quantities, with the latter tending to be smaller as shown by the bin averages (circles). Also shown in Fig. 4 are the bin averages of NMC versus S_C (triangles) and FNOC versus S_C (squares) comparisons over the same time period. The three analyses appear to be very consistent with no systematic differences evident. It is clear in Fig. 4 that the central mooring winds do tend to be low relative to all three of the analyzed wind products at wind speeds above a transition speed $U^T_{S_C}$.

TABLE 2. Primary wind direction comparisons.

x	y	N	$\Delta\theta$	σ	N_1	$\Delta\theta_1$	σ_1
S_C	EC	1179	4.3	30	1051	2.3	13
	NM	597	7.8	27	508	4.6	12
	FN	1225	5.3	44	845	1.1	14
EC	C_0	160	−7.4	43	114	−3.1	14
	C_1	21	7.8	24	18	4.4	15
	C_2	223	1.6	29	181	−0.6	14
	C_3	503	−11.0	32	411	−6.9	13
	C_4	103	−2.1	34	84	−1.3	14
	C_5	126	−0.5	47	99	5.2	14
	M_3	393	−20	—	178	2.1	15
	M_7	34	6.2	57	21	−2.2	16
	P_D	36	−31	23			
S_C	C_0	60	−1.6	34	53	−3.9	13
	C_1	180	7.1	55	133	2.7	14
	C_2	557	1.0	25	504	0.4	14
	C_3	114	0.2	49	102	0.8	12
	C_4	255	2.8	32	217	0.9	13
	C_5	303	5.1	17	287	4.0	11
	M_3	182	10.5	69	108	5.0	15
	M_7	60	12.0	86	31	2.8	15
	S_N	6576	−0.1	39	5673	0.5	11
	P_D	87	−29.3	17			
EC	N_4	1215	−1.0	22	1110	−1.6	11
	N_5	985	3.8	25	888	3.9	12
	N_6	170	9.7	27	146	8.5	11

To determine the transition speed U^T of this and other Ocean Storms comparisons, the data points are fit to two linear segments that meet at U^T. The general form of the fit is

$$U_{10} = U_M \quad U_M \leq U^T$$
$$= AU_M + B \quad U_M > U^T, \qquad (11)$$

where U_M is the observed wind speed shifted to 10 m (Fig. 1) according to (3). The transition speed is varied over a wide range, and for each value the rms distance between the data points and the nearest point on the fitted line (11) is computed. Finally, U^T is taken to be the transition speed for which the rms goodness-of-fit measure is a minimum. The Fig. 4 comparison gives $U^T_{S_C} = 9.05$ m s^{-1}. The fit (11) gives $A_{S_C} = 1.53$ and $B_{S_C} = -4.80$ m s^{-1}.

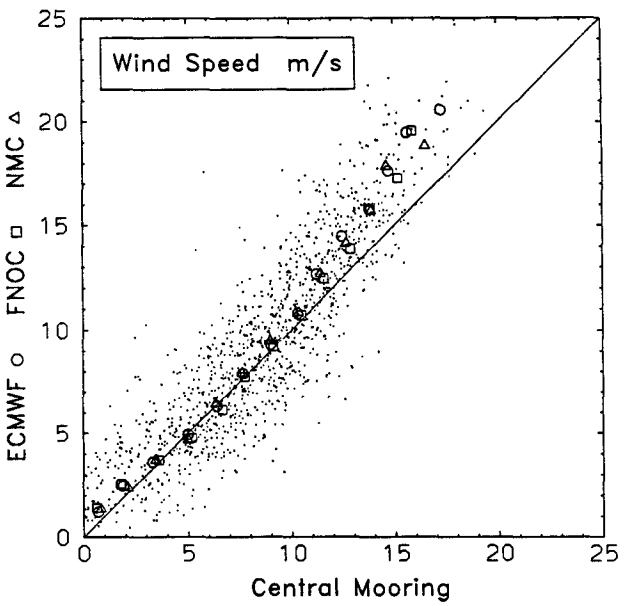

FIG. 4. Scatterplot of interpolated ECMWF wind speeds vs central mooring (S_C) speeds. Bin averages of these data are shown as open circles. Also shown are bin averages from NMC vs S_C (triangles) and FNOC vs S_C (squares) comparisons.

A comparison of hourly average wind speeds from the central and north moorings reveals that, at wind speeds below about 8 m s^{-1}, the north mooring seriously and systematically underestimates the wind speed. The cause of the error is not understood, but any correction would be very nonlinear. At higher wind speeds, however, both moorings give comparable speeds, on average, and the scatter is reasonable given the 60-km separation. Thus, relative to the analyses both moorings give the same high wind speed behavior: $U^T_{S_C} = U^T_{S_N}$, $A_{S_C} = A_{S_N}$, and $B_{S_C} = B_{S_N}$.

A notable feature of this mooring comparison is that from the approximately 9 months of hourly records there are only about 12 reports from each mooring with wind speeds greater than 20 m s^{-1}. The meteorological data from OWS Papa indicates that during the twenty-two September through May periods from 1959 to 1981, the number of 3-hourly observations of wind

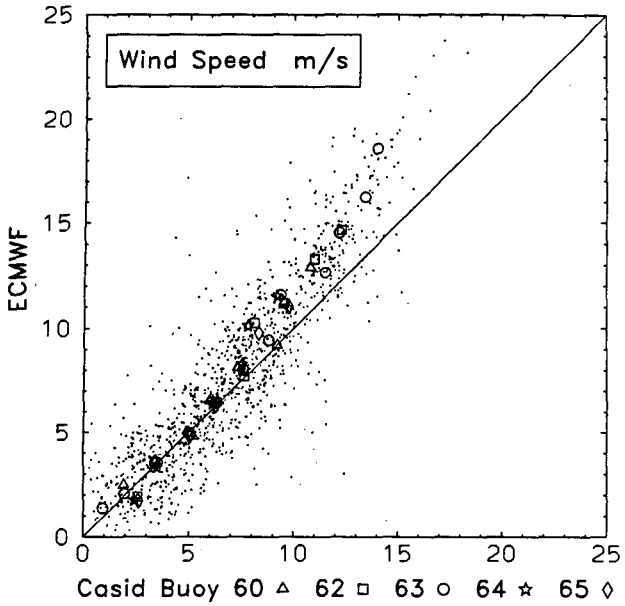

FIG. 5. Scatterplot of interpolated ECMWF wind speeds vs all CASID buoy speeds. Bin averages are shown for the individual comparisons of ECMWF vs C_0 (triangles), C_2 (squares), C_3 (solid circles), C_4 (stars), and C_5 (diamonds).

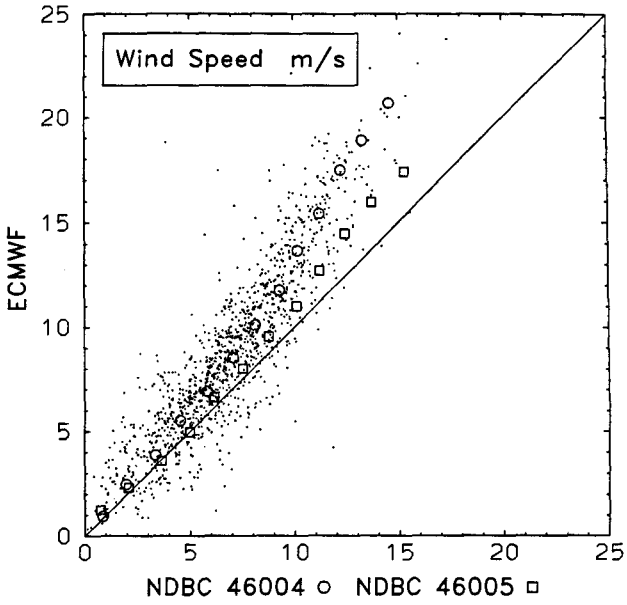

FIG. 6. Scatterplot of interpolated ECMWF wind speeds vs NDBC mooring N_4. Bin averages of these data are shown as open circles. Also shown are bin averages from the ECMWF vs N_5 (triangles) comparison.

speeds greater than 20 m s^{-1} over these nine months ranged from 10 in 1978–1979 to 118 in 1963–1964, with 40 being the median of the 22 values. If it is assumed that hourly observations would have given three times these numbers, then 1987–1988, as measured by the mooring wind speeds, was anomalously calm. However, since hourly averages might tend to be lower than hourly observations, such a year could have occurred. Alternative interpretations are that the Ocean Storms and OWS Papa wind regimes are very different or that the moorings underestimated high winds. There are about 14 occurrences in the Fig. 4 time period of ECMWF 10-m wind speeds in excess of 20 m s^{-1}; the central mooring gives no 6-hour average speeds so high. Thus, the ECMWF data and the central mooring winds corrected according to (11) are more in agreement with the historical record.

Figure 5 is a scatterplot of ECMWF wind speeds and the speeds from the six CASID buoys with bin averages from each. The CASID buoys are consistent. They each give approximately the same bin averages, especially at low wind speeds, where there are more data points and differences are not systematic. However, like the mooring, the drifter winds tend to be relatively low for wind speeds above a transition speed, $U_C^T = 7.25$ m s^{-1}, where subscript C denotes all six CASID buoys. To agree with ECMWF wind speeds, observed CASID wind speeds should be corrected according to (11), but with $A_C = 1.56$ and $B_C = -4.06$ m s^{-1}.

The comparison of ECMWF wind speeds with the NDBC buoys (Fig. 6) is more complicated because these mooring winds tend to be smaller than the analyzed at all wind speeds. This result is somewhat unexpected because the winds from these moorings were presumably assimilated into the analyzed products, whereas winds from Ocean Storms moorings and drifters were not (Table 1). Clearly, wind speeds from NDBC moorings N_4 (circles) and N_5 (squares) do not agree with each other. One procedure for correcting these NDBC winds to agree with ECMWF is to first apply a gain factor of $G_{N_4} = 1.20$ and $G_{N_5} = 1.05$, respectively, to all the winds in each dataset. Such corrections sometimes need to be applied because of calibration errors or instrument problems such as overspeeding (Izumi and Barad 1970; Busch and Kristensen 1976). For each mooring, the gain is the ratio of the average ECMWF speed to the average mooring speed over a bin bordered by lines perpendicular to the 1:1 line at 0 and 8 m s^{-1} along the line. Following these gain corrections both sets of NDBC mooring data are consistent and behave relative to ECMWF in the fa-

TABLE 3. Summary of wind speed corrections.

Platforms	z_a (m)	U^T (m s^{-1})	A	B (m s^{-1})	Gain
CASID	3.0	7.25	1.56	−4.06	
S_C, S_N	4.5	9.05	1.53	−4.80	
N_4	5.0	9.20	1.40	−3.68	1.20
N_5	5.0	9.20	1.40	−3.68	1.05

miliar fashion seen in Figs. 4 and 5. The transition speed, $U_N^T = 9.20$ m s^{-1}, where subscript N denotes all NDBC moorings, is the highest. A composite fit (11) gives $A_N = 1.40$ and $B_N = -3.68$ m s^{-1}.

The above corrections are summarized in Table 3. There is a very distinct trend for the transition speed to increase with the measurement height. Wind speed errors in the ECMWF data should not lead to this result. However, flow distortion of the wind profile by surface waves could because wave heights tend to increase with wind speed. As the wind speed and wave heights increase, the profile distortion would extend to higher levels. Thus, when 10-m shifted wind speeds from two anemometers at different low levels are compared, the high speeds from the lower anemometer should tend to be smaller than those from the higher one. Such a tendency is evident when CASID buoy wind speeds from measurements at 3.0 m are compared to central mooring winds from measurements at 4.5 m. For S_C speeds greater than about 9 m s^{-1}, all three CASID buoys tend to give smaller speeds. The ECMWF comparisons indicate that at these speeds both the S_C and CASID winds should be corrected, but the latter more so.

The Ocean Storms WOTAN data provide further evidence that the mooring winds are too low at high wind speed. The FASINEX noise to wind speed comparisons of Vagle et al. (1990) also hint at the presence of some wave distortion of the wind profile at winds above 10 m s^{-1}. The FASINEX mooring winds near 15 m s^{-1} are systematically low compared to the extrapolated linear calibration that was used to convert the Ocean Storms acoustic noise. However, any distorted FASINEX data, although not plentiful, would have influenced the calibration fits somewhat. The net result would be to make the Ocean Storms WOTAN winds somewhat too small. Accordingly, Vagle et al.'s (1990) plot of WOTAN versus central mooring wind speeds shows a tendency for relatively low S_C winds at the higher wind speeds, which is similar to that seen in Fig. 4. However, the S_C corrected winds would tend to be somewhat higher than the WOTAN winds.

Anemometer performance is unlikely the cause of the high wind speed behavior relative to analyses because propellers and rotors display similar behavior but have very different performance characteristics. It is well known, for example, that horizontally rotating anemometers such as cups and Savonius rotors can tend to overspeed because of the inertia of the rotating sensor and platform motion (Kaganov and Yaglom 1976). However, such sensors have the advantage on tilting platforms of not responding to the cosine of the angle of attack as do propellers (MacCready 1966). Notwithstanding the paucity of data, the Savonius rotors of the Marisonde buoys appear to overspeed by about 10%, according to the Fig. 7 comparison with ECMWF at speeds between U^L and about 8 m s^{-1}. At higher speeds a further correction for the wave distortion appears to be needed, but since the two corrections tend

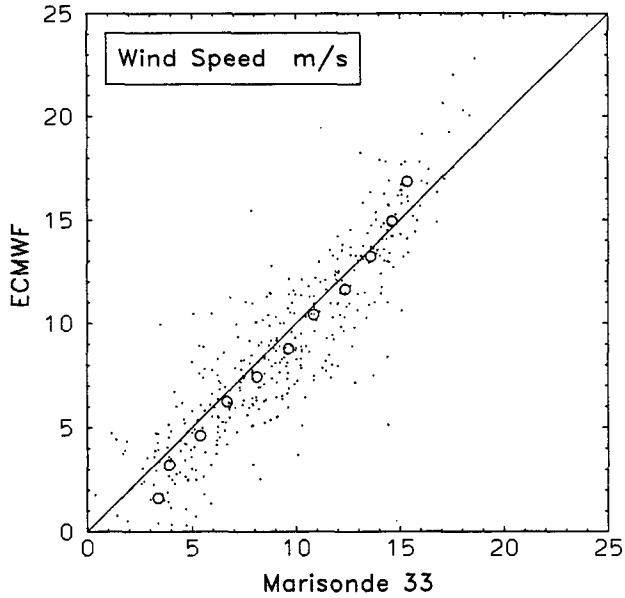

FIG. 7. Scatterplot of interpolated ECMWF wind speeds vs Marisonde buoy M_3 wind speeds. Bin averages are shown as open circles.

to compensate, the ECMWF and M_3 wind speeds are in good agreement around 14 m s^{-1}. A similar comparison of *Parizeau* drifter winds indicates an overspeeding of its cup anemometer by about 5%. Again, at high winds ECMWF and P_D speeds agree quite well because of the compensating errors. As illustrated by Fig. 7, it can be difficult to interpret a comparison, especially over a narrow wind speed range, when corrections are needed for competing effects.

The *Parizeau* ship cup and vane system winds, P_C, were measured above any suspected wave influence. Since these winds were continuously recorded, they could have been a useful local reference, overspeeding notwithstanding. However, it appears as if they have gross errors of unknown origin, making them unsuitable for such a purpose. This situation was revealed by comparing these winds to speeds from the *Parizeau* propeller anemometers, P_M and P_B. By selecting data from one propeller or the other depending on the relative wind direction, flow distortion by the ship can be minimized, and a relatively reliable composite wind dataset compiled. Relative to this dataset, the P_C wind behavior was very erratic. They give wind speeds of 7–8 m s^{-1} when the propeller speeds are less than 2 m s^{-1}. Visual observations confirm the calm conditions (L. Zedel 1988, personal communication). Conversely, the propeller speeds sometimes exceed the P_C speeds by more than 3 m s^{-1}. Such discrepancies, especially in collocated wind measurements, are not acceptable.

Additional support for correcting the mooring and drifter winds is provided by the performance of one-

dimensional ocean models. Model simulations of Ocean Storms wind events have been carried out by Large and Crawford (1995). They find that such a numerical model is able to reproduce the observed ocean responses to several storms if it is forced with corrected CASID buoy winds. One particular model is based on known boundary layer physics as parameterized by a nonlocal vertical diffusivity and is described and verified by Large et al. (1994). Two examples of simulated versus observed response are plotted in Fig. 8.

The change in kinetic energy, ΔIKE_m, represents the increase over the duration of a storm in the kinetic energy of inertial currents integrated over the upper-mixed layer. The change in the potential energy over the duration of a storm, $\Delta\text{PE}_{\text{mix}}$, has been corrected for surface buoyancy fluxes and advection, so that it represents the change due solely to the vertical exchange of heat and salt between the mixed layer and the deeper, colder thermocline. Details of how these responses were computed from Ocean Storms observations are given in Large and Crawford (1995). Also shown in Fig. 8 are these responses compared to observations when the model is forced with uncorrected 10-m winds. The weaker winds are able to produce only a small fraction to the observed energy increases. In these cases the forced mixed layer inertial currents are much too weak, and the change in mixed layer temperature is much too small. Large and Crawford (1995) also used both a second-order closure model (Mellor and Yamada 1982) and a bulk mixed layer model (Price et al. 1986) to simulate these Ocean Storms responses. Both of these models produced somewhat weaker responses, and therefore, if forced with the uncorrected winds, they would compare even more poorly to observations.

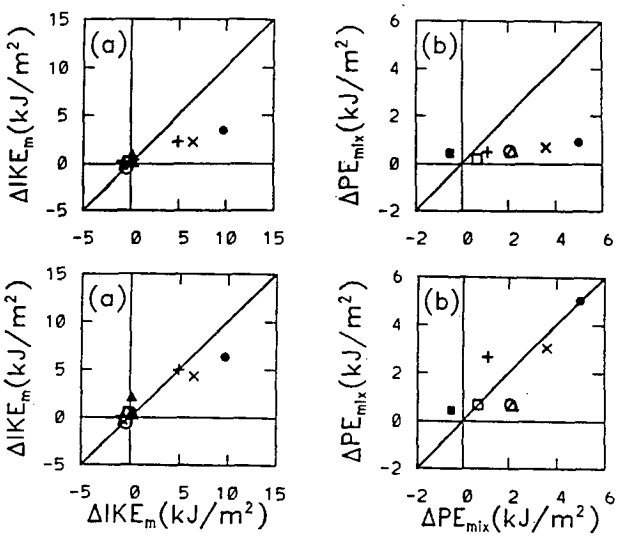

FIG. 8. A comparison of the observed ocean responses: (a) change in mixed layer kinetic energy ΔIKE_m and (b) change in potential energy due to vertical mixing ΔPE_v vs simulated responses (ordinates) from an upper-ocean numerical model forced with both uncorrected (upper panels) and corrected (lower panels) winds from collocated CASID buoys. Symbols refer to different storm events.

6. The low-level wind profile

The high wind speed corrections of Table 3 can be interpreted as accounting for distortion of the low-level wind profile by surface waves. However, to properly correct for this effect in general, it is necessary to know the form of the functions $\Omega(\xi)$ in (5) and hence $\chi(\xi)$ in (4). In addition, a proper wave height parameter, h, needs to be found. To at least obtain crude approximations to these functions from the corrections found for Ocean Storms, the wind speed is used to approximate a wave height:

$$h = 2\sqrt{2}\sqrt{E},$$

where

$$E = 3.64 \times 10^{-3} U_{10}^4 g^{-2} \qquad (12)$$

is the total variance under the Pierson and Moskowitz (1964) wave spectrum, and g is gravitational acceleration (SWAMP Group 1985). This is just the height of a monochromatic wave train with energy E. For a given value of $\xi_a = z_a/h$, three values of h, and hence of U_{10} by inverting (12), can be computed, one for each of the three values of z_a in Table 3. The values of U_{10} then give u^* from (8). For each of these three datasets there is a transition value, $\xi^T = z_a/h^T$, where h^T is the wave height at the transition speed U^T, as given by (12).

Since high winds generally produce near-neutral stability conditions [$\phi(\zeta) = 1$, $\psi(\zeta) = 0$], (5) at heights z_s and z_a gives

$$U_{10} - U(z_a) = \frac{u^*}{\kappa}\left[\ln\frac{z_s}{z_a} + \Omega(\xi_a) - \Omega(\xi_s)\right], \qquad (13)$$

where $\xi_s = (z_s/h)$. Similarly, the roughness length as measured, z_m, can be eliminated from (3) to give

$$U_M - U(z_a) = \frac{u_m^*}{\kappa}\ln\frac{z_s}{z_a}, \qquad (14)$$

where u_m^* is the friction velocity determined from (8) using U_M. Eliminating $U(z_a)$ from (13) and (14) yields

$$\Omega(\xi_a) = \Omega(\xi_s) + \left(\frac{u_m^*}{u^*} - 1\right)\ln\frac{z_s}{z_a} + \frac{\kappa}{u^*}(U_{10} - U_M). \qquad (15)$$

For each dataset, $(U_{10} - U_M)$ can be expressed as a function of U_{10} using (11). At large values of $\xi_a \geq \xi^T$, wave distortion is not observed, implying $\Omega(\xi_a) = \Omega(\xi_s) = \Omega_L$, where Ω_L is a constant. If a value for Ω_L is assumed, then (15) can be solved for $\Omega(\xi_a)$ by starting at large ξ_a (low winds) and bootstrapping to lower values (higher winds). The point at which the

resulting curve becomes zero defines $\xi_r = z_r/h$ because (5) demands $\Omega(\xi_r) = 0$. The wind–wave tank observations of Tseng et al. (1992) show that the reference height where the wind speed goes to zero ranges from about 0.2 to 0.4 times the wave amplitude. The wave amplitude should be about 2 h, so assuming this reference height and z_r are similar, ξ_r should be in the range 0.1–0.2.

The CASID, central mooring, and NDBC datasets have each been used to give $(U_{10} - U_M)$ as a function of U_{10} through (11), and hence of h through (12) and of ξ_a. The three resulting estimated functions $\Omega(\xi)$ are shown in Fig. 9a. For each a value of $\Omega_L = -6.0$ was chosen to put ξ_r near 0.1. However, shifting wind heights do not depend on this choice, because only differences in Ω are involved (13). All three datasets give comparable results (Fig. 9a). The functions are greater than Ω_L for all $\xi < \xi^T$, where ξ^T equals 3.28, 3.15, and 3.39, respectively. The curves are piecewise linear because of the linear corrections (11).

The function $\chi(\xi)$ is related to the derivative of $\Omega(\xi)$ with respect to ξ through (5):

$$\chi(\xi) = 1 - \xi \frac{d\Omega}{d\xi}. \tag{16}$$

Thus, $\chi(\xi)$ could be computed from the derivatives of the curves in Fig. 9a. However, the curves would first need to be smoothed to eliminate the discontinuous first derivatives, otherwise the $\chi(\xi)$ functions would also be discontinuous.

Alternatively, estimates of $\chi(\xi)$ can also be found from the discrete wind speed gradients,

$$\nabla_z U = \frac{U_{10} - U(z_a)}{(z_s - z_a)} = \frac{U_{10} - U_M + u_m^* \kappa^{-1} \ln(z_s/z_a)}{(z_s - z_a)}. \tag{17}$$

A discrete, neutral stability form of (4) is just

$$\chi(\xi_a) = \frac{\kappa z_i}{u^*} \nabla_z U. \tag{18}$$

The discrete gradient (17) is only an approximation to the gradient at $\xi_a = z_a/h$, but the proper choice of z_i can ensure that $\chi(\xi_a) = 1$ at values of $\xi_a > \xi^T$, where the comparison results find $U_M = U_{10}$; namely,

$$z_i = \frac{u^*}{u_m^*} \frac{(z_s - z_a)}{\ln(z_s/z_a)}. \tag{19}$$

Figure 9b shows $\chi(\xi)$ from (17), (18), and (19) as derived from the CASID, central mooring, and NDBC wind corrections. When $u^* = u_m^*$, the respective values of z_i are 5.8, 6.9, and 7.2 m. These three estimates of $\chi(\xi)$ are in general agreement. They indicate that for $\xi = 1$, the wind speed gradient is about three times as large as would be expected in the absence of surface waves. It is because the wind speed decreases so much faster with height in the presence of waves that z_r can be orders of magnitude greater than z_0 as indicated in Fig. 1.

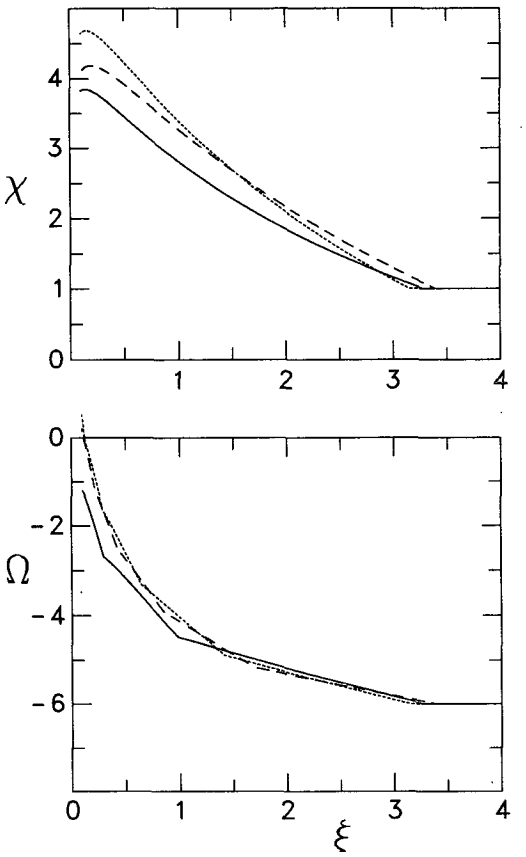

FIG. 9. (a) The function $\Omega(\xi)$ as determined from the corrections to the CASID wind speeds (solid curve), to the central mooring speeds (dotted curve), and to the gain-corrected NDBC wind speeds (dashed curve). (b) Same as Fig. 9a except for the function $\chi(\xi)$.

7. Discussion and conclusions

Low-level Ocean Storms wind measurements at high speeds were smaller, on average, than both the analyzed wind products and the WOTAN winds. This effect appeared to be enhanced at lower measurement heights. Thus, it does appear as if the surface wave influence on the wind profile did extend up to the levels of Ocean Storms wind measurements. These heights are much higher than the theoretical study Janssen (1989) predicts for the extent of surface wave influence. There does not appear to have been any surface wave effects on wind direction. Wind directions as measured by sensors at various heights generally agreed with each other to within expected errors. The most notable exception were the directions from the Marisonde drifters, so their technique of using a hull-mounted fin to align the hull into the wind, then mea-

suring the orientation of its hull with a compass may not be reliable. Better results were obtained from systems with an additional wind-vane measurement, and in the case of the CASIDs, conditional sampling. Contamination of the Marisonde winds during periods of excessive platform activity may have contributed to the large overspeeding correction (10%).

The consistency of the CASID buoy winds with one another, the agreement between the analyses and various wind speed measurements at low wind speeds, and the high wind speed agreement between winds from the north and central moorings all suggest that the central mooring and CASID winds, as measured at the anemometer heights, were essentially correct. This result is in accord with Weller et al. (1983), who concluded that propeller-vane anemometers perform well on active ocean platforms. However, to compare wind speeds observed at different heights and to estimate surface wind stress, it is not enough to have correct measurements. It is also necessary to properly shift these winds to the common reference height, z_s. The simplest means of doing so for Ocean Storms observations is to apply the corrections summarized in Table 3 to 10-m speeds from (3). However, this procedure essentially references all the measurements to the analyzed wind speeds mainly from ECMWF but also from NMC and FNOC. However, these products cannot be regarded as a standard, at least globally, because of known systematic errors in the tropics (Trenberth et al. 1990) and over midlatitude western basins (Kent et al. 1993; P. K. Taylor 1992, personal communication). There are also discrepancies between the ECMWF and NMC analyses (Trenberth and Olson 1988). Fortunately, the 10-m wind analyses at the western basin site of Ocean Storms are consistent (Fig. 4) and appear to be accurate at least at low wind speeds (Figs. 4 and 5).

The apparent wave influence is profound. A 10-m central mooring wind of 17 m s^{-1} becomes more than 20 m s^{-1} after correction. The greater speed and higher drag coefficient [(7) and (8)] result in about a 40% higher wind stress (6). Only with the higher stresses were numerical ocean models able to reproduce observed Ocean Storms responses to high wind events (Fig. 8). In accord is the D'Asaro et al. (1995) result that the magnitude of observed energetic (0.35–0.7 m s^{-1}) inertial motions can be predicted from the higher stresses.

Other studies that make use of wind speeds from low-level anemometers should consider whether or not profile distortion by surface waves needs to be considered. For example, Halpern et al. (1994) show monthly mean wind speeds from the Special Sensor Microwave Imager (SSMI) on board a DSMP satellite versus comparable winds from surface moorings. The behavior is similar to Figs. 5, 6, and 7. Above about 8 m s^{-1} the buoy speeds tend to be smaller than those derived from SSMI. Quantitatively, the two comparisons should differ because Halpern et al. (1994) show monthly means, because they use many different buoys, and because the SSMI model function is based largely on empirical relations with buoy winds (Wentz 1992). Also, Weller et al. (1983) intercompared wind measurements from nine anemometers mounted on various buoy types at heights ranging from 2.0 to 7.7 m during the Joint Air–Sea Interaction Experiment. Their examination raised doubts about the performance of the anemometers, the processing, and buoy motion. Even though the wind speeds were always less than 10 m s^{-1}, some of the peculiar behavior noted in the comparisons could have been due to wave distortion of the wind profile. For example, a comparison of winds observed at 7.7 and 3.5 m is similar to Fig. 7, where both overspeeding and wave distortion appear to be competing.

General corrections to be applied to any wind measurement can be approximated from the $\Omega(\xi)$ function of Fig. 9a. However, the Ocean Storms data were far from ideal for determining this function. A more suitable dataset would include measurements from identical wind sensors at several heights from about 2 m to more than 10 m at the same site. In Ocean Storms the direct wind measurements spanned only from 3.0 to 5.0 m in height, utilized different anemometers and processing systems, and were often far apart. It would also be preferable to have direct measurements of the wind stress, and hence u^* and of wave height, rather than to have to rely on empirical relationships such as (8) and (12). Thus, the Ocean Storms results (Fig. 9) are at best crude approximations to $\Omega(\xi)$ and $\chi(\xi)$ but should be better than ignoring wave effects. They probably reveal the general features of these functions and should be useful in designing a proper observational program.

The traditional roughness length z_0 is derived from measurements in the atmospheric surface layer. Over solid surfaces it has been related to the size and distribution of the roughness elements (Wu 1973; Jackson 1981), implying that (2) is valid down to order z_0. This is not true over surface water waves, where z_0 is not related to the height where the wind matches U_0. In accord with Krugermeyer et al. (1978), the physics of (2) appear to hold only above about three wave heights, where $\chi = 1$ (Fig. 9b) and Ω is constant (Fig. 9b). For some distance below the marine surface layer, (4) appears to hold, so that the wind profile follows the solid trace of Fig. 1, at least to the lowest height (z_a = 3.0 m) and greatest wind speed (25 m s^{-1}) of the Ocean Storms dataset. Corresponding values are h = 10.9 m and $\xi = 0.28$. Beyond these extremes, knowledge of the wind profile is an extrapolation into regimes where other physics may become important, such that the wind profile deviates away from that given by (5), too. The nature of the marine wind profile at these heights is beyond the scope of this present study and perhaps better addressed by wind/wave tank studies, such as those of Tseng et al. (1992).

Acknowledgments. The generous support of the U.S. Office of Naval Research (N00014-89-J-1215) throughout the planning, field, and analysis phases of Ocean Storms is gratefully acknowledged. Personal support for GBC was received from the U.S. Office of Naval Research (N00014-91-F-0003) and the Advanced Study Program at the National Center for Atmospheric Research. We are indebted to all those who contributed to the Ocean Storms wind measurement program. Particular appreciation is extended to T. Anderson, N. Daniault, R. Davis, G. McBean, P. Niiler, and L. Zedel, and to NDBC for maintaining the offshore meteorological buoys.

REFERENCES

Busch, N. E., and L. Kristensen, 1976: Cup anemometer overspeeding. *J. Appl. Meteor.*, **15,** 1328–1332.

Chalikov, D., and V. Makin, 1991: Models of the wave boundary layer. *Bound.-Layer Meteor.*, **56,** 83–99.

Danard, M., 1980: A note on estimating the height of the constant flux layer. *Bound.-Layer Meteor.*, **20,** 397–398.

D'Asaro, E. A., P. Van Meurs, and P. P. Niiler, 1995: Upper-ocean inertial currents forced by a strong storm. Part I: Data and comparisons with linear theory., *J. Phys. Oceanogr.*, **25,** 2909–2936.

Deardorff, J. W., 1968: Dependence of air–sea transfer coefficients on bulk stability. *J. Geophys. Res.*, **73,** 2549–2557.

Dittmer, K., 1977: The hydrodynamic roughness of the sea surface at low wind speeds. *Meteor.*, **12,** 10–15.

ECWMF, 1993: The description of the ECMWF/WCRP level III-A global atmospheric data archive. Tech. Attachment, ECMWF, Reading, U.K., 49 pp.

Gilhousen, D. B., E. A. Meindl, M. J. Changery, P. L. Franks, M. G. Burgin, and D. A. McKittrick, 1990: Climatic summaries for NDBC buoys and stations, update 1. National Data Buoy Center, NSTL, MS, 10 pp.

Halpern, D., A. Hollingsworth, and F. Wentz, 1994: Global surface wind speeds from operational forecast-analysis and satellite. *J. Atmos. Oceanic Technol.*, **11,** 779–788.

Högström, U., 1988: Non-dimensional wind and temperature profiles in the atmospheric surface layer: A re-evaluation. *Bound.-Layer Meteor.*, **42,** 55–78.

Hollingsworth, A., D. B. Shaw, P. Lonnberg, L. Illari, K. Arpe, and A. J. Simmons, 1986: Monitoring of observations and analysis quality by a data assimilation system. *Mon. Wea. Rev.*, **114,** 861–879.

Izumi, Y., and M. L. Barad, 1970: Wind speeds as measured by cup and sonic anemometers and influenced by tower structure. *J. Appl. Meteor.*, **9,** 851–856.

Jackson, P. S., 1981: On the displacement height in the logarithmic velocity profile. *J. Fluid Mech.*, **111,** 15–25.

Janssen, P. A. E. M., 1989: Wind-induced stress and drag of air flow over sea waves. *J. Phys. Oceanogr.*, **19,** 745–754.

Jones, W. L., L. C. Schroeder, D. H. Boggs, E. M. Bracalente, R. A. Brown, G. J. Dome, W. J. Pierson, and F. J. Wentz, 1982: The *Seasat-A* satellite scatterometer: The geophysical evaluation of remotely sensed wind vectors over the ocean. *J. Geophys. Res.*, **87,** 3297–3317.

Kaganov, E. I., and A. M. Yaglom, 1976: Errors in wind-speed measurements by rotation anemometers. *Bound.-Layer Meteor.*, **10,** 15–34.

Kent, E. C., P. K. Taylor, B. S. Truscott, and J. S. Hopkins, 1993: The accuracy of voluntary observing ship's meteorological observations. *J. Atmos. Oceanic Technol.*, **10,** 591–608.

Krugermeyer, L., M. Gruenewald, and M. Dunckel, 1978: The influence of sea waves on the wind profile. *Bound.-Layer Meteor.*, **14,** 403–414.

Large, W. G., 1979: The turbulent fluxes of momentum and sensible heat over the open sea during moderate to strong winds. Ph.D. thesis, University of British Columbia, 180 pp.

——, and S. Pond, 1981: Open ocean momentum flux measurements in moderate to strong winds. *J. Phys. Oceanogr.*, **11,** 324–336.

——, and G. B. Crawford, 1995: Observations and simulations of upper-ocean response to wind events during the Ocean Storms Experiment. *J. Phys. Oceanogr.*, **25,** 2831–2852.

——, J. C. McWilliams, and S. Doney, 1994: Oceanic vertical mixing: A review and a model with a nonlocal boundary layer parameterization. *Rev. Geophys.*, **32,** 363–403.

Lorenc, A. C., 1981: A global three-dimensional multivariate statistical interpolation scheme. *Mon. Wea. Rev.*, **109,** 701–721.

Lumley, J. A., and H. A. Panofsky, 1964: *The Structure of Atmospheric Turbulence.* Wiley and Sons, 239 pp.

MacCready, P. B., 1966: Mean wind speed measurements in turbulence. *J. Appl. Meteor.*, **5,** 219–225.

Mellor, G. L., and T. Yamada, 1982: Development of a turbulence closure model for geophysical fluid problems. *Rev. Geophys. Space Phys.*, **20,** 851–875.

Pierson, W. J., Jr., and L. Moskowitz, 1964: A proposed spectral form for fully developed wind seas based on the similarity theory of S. A. Kitaigorodskii. *J. Geophys. Res.*, **69,** 5181–5190.

Price, J. F., R. A. Weller, and R. Pinkel, 1986: Diurnal cycling: Observations and models of the upper ocean response to diurnal heating, cooling and wind mixing. *J. Geophys. Res.*, **91,** 8411–8427.

——, ——, C. M. Bowers, and M. G. Briscoe, 1987: Diurnal response of sea surface temperature observed at the Long-Term Upper Ocean Study (34°N, 70°W) in the Sargasso Sea. *J. Geophys. Res.*, **92,** 14 480–14 490.

SWAMP Group, 1985: *Ocean Wave Modeling.* Plenum, NY, 256 pp.

Tennekes, H., 1973: The logarithmic wind profile. *J. Atmos. Sci.*, **30,** 234–238.

Trenberth, K. E., and J. G. Olson, 1988: An evaluation and intercomparison of global analyses from the National Meteorological Center and the European Centre for Medium-Range Weather Forecasts. *Bull. Amer. Meteor. Soc.*, **69,** 1047–1057.

——, W. G. Large, and J. G. Olson, 1990: The mean annual cycle in global ocean wind stress. *J. Phys. Oceanogr.*, **20,** 1742–1760.

Tseng, R-S., Y.-H. L. Hsu, and J. Wu, 1992: Methods of measuring wind stress over a water surface—Discussions of displacement height and von Kármán constant. *Bound.-Layer Meteor.*, **58,** 51–68.

Vagle, S., W. G. Large, and D. M. Farmer, 1990: An evaluation of the WOTAN technique of inferring oceanic winds from underwater ambient sound. *J. Atmos. Oceanic Technol.*, **7,** 576–595.

Weller, R. A., R. E. Payne, W. G. Large, and W. Zenk, 1983: Wind measurements from an array of oceanographic moorings and from F/S Meteor during JASIN 1978. *J. Geophys. Res.*, **88,** 9689–9705.

——, D. L. Rudnick, R. E. Payne, J. P. Dean, N. J. Pennington, and R. P. Trask, 1990: Measuring near-surface meteorology over the ocean from an array of surface moorings in the subtropical convergence zone. *J. Atmos. Oceanic Technol.*, **7,** 85–103.

Wentz, F., 1992: Measurement of oceanic wind vector using satellite microwave radiometers. *IEEE Trans. Geosci. Remote Sens.*, **30,** 960–972.

Wu, J., 1973: Flow in turbulent wall layer over uniform roughness. *J. Appl. Mech.*, **40,** 863–867.